Single-Shot Pulsed-LiDAR SPAD Sensor with on-chip Peak Detection for Background Rejection

Alfonso Incoronato, *Graduate Student Member, IEEE*, Iris Cusini, Klaus Pasquinelli, and Franco Zappa, *Senior Member, IEEE*

***Abstract*—In recent years, direct Time-of-Flight techniques have been exploited with single-photon detectors to provide long distance ranges and high-frame rates measurements. Detectors based on Silicon Photon Multipliers commonly collect repetitive laser shots to reconstruct a histogram of the TOF of returning pulsed-laser photons, so to discriminate between signal, background light, and detector noise. Instead of performing multi-shot measurements, we propose a single-shot technique capable to provide just one useful TOF per laser pulse, corresponding to the returning peak signal with the highest number of concurrent photons. In this way, ambient background photons and dark counts are rejected, being mostly randomly distributed over time compared to the laser pulse photons. Therefore, there is no need for repetitive laser shots, neither to acquire and store multiple TOFs, nor to post-process any TOF histogram, since each laser shot can provide the useful distance information. We present a sensor chip based on a pixel with 272 SPADs, which concurrently provide an analog signal to a peak detector triggering a multi-hit TDC each time the number of concurrent photons exceeds the previous peak. We report preliminary tests up to 25 m, rejecting 60 klux solar background, with $>$ 95% single-shot success ratio.**

***Index Terms*—Single photon avalanche diode (SPAD), silicon photo multiplier (SiPM), light detection and ranging (LiDAR), time-of-flight (TOF), telemetry, distance ranging.**

I. Introduction

LIGHT Detection And Ranging (LiDAR) systems find application in many fields requiring either object recognition or remote sensing, thanks to their capability of reconstructing 3D scenes with sub-centimeter resolution. Among different 3D ranging techniques, such as stereo-vision and structured light projection, Time-of-Flight (TOF) methods are the most promising for long-range measurements, by measuring the return light "echo" from the target [1]. In direct Time-of-Flight (dTOF) ranging, a pulsed laser illuminates the scene and the backscattered light is detected by a photodetector, which triggers a Time-to-Digital Converter (TDC) to measure the TOF delay between light excitation and returning echo.

Manuscript received December 11, 2021; revised February 18, 2022, April 11, 2022, and May 31, 2022; accepted June 1, 2022. Date of publication June 13, 2022; date of current version June 24, 2022. *(Corresponding author: Alfonso Incoronato.)*

The authors are with the Dipartimento di Elettronica, Informazione e Bioingegneria (DEIB), Politecnico di Milano, 20133 Milano, Italy (e-mail: alfonso.incoronato@polimi.it; iris.cusini@mail.polimi.it; klaus.pasquinelli@polimi.it; franco.zappa@polimi.it).

Color versions of one or more figures in this article are available at https://doi.org/10.1109/JSTQE.2022.3180687.

Digital Object Identifier 10.1109/JSTQE.2022.3180687

In order to reconstruct the 3D target scene, it is possible to employ either a flood illumination and a 2D pixel array (flash LiDAR) or to scan a light spot (or a light line) across the scene (scanning LiDAR) and using a single-pixel (or a 1D linear array) detector, thus relaxing imager's spatial resolution requirements. Commonly, LiDAR systems use a pulsed laser and each detector's pixel measures the TOF from each spot of the target scene. Ideally, flash-LiDAR systems could acquire the entire scene in a single laser shot, but the laser pulse energy required to cover a wide field-of-view (FOV) often exceeds the eye-safety limits. Therefore, flash LiDAR is usually limited to few tens of meters in high background noise environment due to laser power constraints [2]–[4], while scanning LiDAR reaches longer distances, but with reduced FOV and a frame rate limited by the scanning process.

Automotive advanced driver assistance systems (ADAS) and autonomous driving in vehicles and drones require fast 3D monitoring of the scene to manage different traffic situations and hazards, often with few centimeters resolution, hundreds of meters ranges, and short computation time. Moreover, the detector must have wide dynamic range, since the laser echo decreases with the square of the distance, targets' reflectivity is quite variable, and background light is usually high.

Single-Photon Avalanche Diodes (SPADs) are acquiring increased popularity over Avalanche Photo Diodes (APDs) in LiDAR applications [5]. SPAD's avalanche multiplication process results in a "digital" operation providing single-photon sensitivity and immunity from electronic noise, which instead affects APD's front-end. Silicon SPADs (sensitive up to 1000 nm wavelength) can be employed at ambient temperature, have low Dark Counting Rate (DCR, the intrinsic noise) and can be integrated together with on-chip analog and digital electronics, for TOF measurements and distance pre-processing. InGaAs/InP SPADs extend the sensitivity up to 1.7 μm wavelength, but require cooling and show a quite higher DCR [6], [7]. Unfortunately, the dead-time needed to quench the SPAD after each triggering and reset it back to operation (few tens of nanosecond for Silicon SPADs, up to microseconds for InGaAs ones) limits the maximum photon rate. Moreover, since the SPAD (through its quenching and reset circuitry) provides a digital pulse if triggered by at least one photon or any other generation process (e.g., DCR), it is not possible to discriminate between one or more concurrent photons. Eventually, the triggering probability per SPAD must be kept low enough to avoid "detector's pile-up" [8], above all in high background environments, so small optical

apertures and higher number of SPADs per pixel (i.e., per target spot) [9] are preferred.

Due to spurious triggering, such as the intrinsic DCR and the presence of background light, the distance of a target cannot be retrieved by a single TOF measurement. Usually, the laser shot and the TOF acquisition are repeated many (from tens to thousands) times, in order to accumulate a histogram of TOF measurements: the peak usually identifies the useful laser echo, other lower peaks could come from spurious multiple reflections, while the baseline results from the random time-distribution of DCR events and background photons. When the timing electronics is able to measure just one TOF per laser shot, only the first triggering event will be recorded, while all subsequent ones will be lost. This "electronics' pile-up" [8] causes stronger histogram distortion the higher the probability of false events gets (e.g., at increasing background or target distance). Therefore, in noisy environments, a multi-hit TDC and storage able to record multiple TOF data (both false and true events) per each laser shot is needed.

In order to reject background and limit pile-up, wavelength filtering is a must, but it is often not enough and further techniques can be exploited both at the detector side and in post-processing. Since events due to DCR and ambient photons are not correlated in time, while photons belonging to the laser pulse are concurrent, it is possible to acquire the TOF only when a given minimum number of photons are detected by a set of SPADs within a time duration equal to the laser width. Some LiDAR systems employ a silicon photomultiplier (SiPM), comprising of multiple SPADs connected to a common analog output, which produces an overall current signal given by the sum of the avalanche current pulses of the fired SPADs [10], [11]. An analog discriminator senses when a given threshold is exceeded, so to trigger a TDC. Such a threshold should trade-off between a high value to minimize false triggering (i.e., TOF measurements due to noise or ambient background) and a low value to maximize sensitivity.

Herein we present a novel technique and pixel design specifically developed for automotive LiDAR applications in high background environments, where an innovative peak detection allows to identify the signal peak while being insensitive to other spurious events, with no need to set a coincidence threshold and no need to acquire more TOF data per laser shot. The peak detector tracks the number of concurrent photons and stores the TOF of just the highest peak (i.e., with the highest number of coincident photons) per frame (i.e., per laser shot). In this way, only the highest signal peak is time-stamped, with no need to collect a histogram, neither to store more TOF data per frame, nor to perform post-processing. The sensor can operate in single-shot regime so to avoid laser repetitions on the same point of the scene, hence increasing the scene acquisition rate in scanning single-spot LiDAR.

Section II briefly compares the background rejection methods commonly employed in LiDAR systems with the proposed technique. Section III describes in detail the chip architecture and each block, with the design choices. Section IV discusses the experimental characterization and the validation of the background rejection technique. Eventually, Section V summarizes the achieved performance.

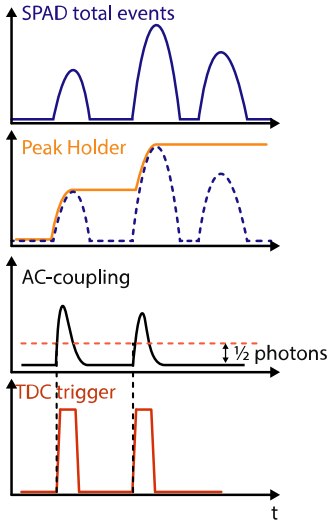

Fig. 1. Proposed peak detection method.

II. Peak Detection Method

As introduced in Section I, the main issue in dTOF automotive LiDAR systems is the presence of strong background light; hence, it is not enough to measure the TOF of just the first detected event, as it is usually done in other applications such as Time-Correlated Single Photon Counting (TCSPC) [12]. One common strategy for background rejection is to set a threshold on the minimum number of coincident photons needed to trigger the TDC and to measure the TOF. In case of an analog SiPM, when the total output current amplitude outreaches the given threshold, a TDC measures the TOF and stores it into a memory cell. An adjustable threshold allows the system to adapt to different background and signal intensities. However, in automotive scenarios, both may change by several orders of magnitude, due to variation in target reflectivity, incidence angle on the illuminated objects, atmospheric conditions, etc. Hence, the system must measure the background light intensity so to set the threshold accordingly.

In analog SiPMs, the problem can be strongly attenuated by filtering out the low-frequency components from the signal. In this way, the threshold should be set in accordance with the background variance. The latter, however, being equal to the background mean value, still depends on target reflectivity and incidence angle, which can significantly vary from point to point in the scanned scene.

Another background rejection strategy consists instead in identifying all peaks in the echo signal, with a width comparable to the laser pulse one. However, this method usually requires fast Analog-to-Digital Converters (ADCs) to acquire the whole photocurrent waveform with sub-nanosecond sampling rate, and then post-processing to identify the laser peak and compute its TOF. Such a sensor would be expensive and communication between detector, ADC and processor requires high data-rates [13], as for example in [14], [15].

We propose to overcome all these issues with the different sensing of the detected signal shown in Fig. 1. An array of SPADs provides an analog signal waveform proportional to the

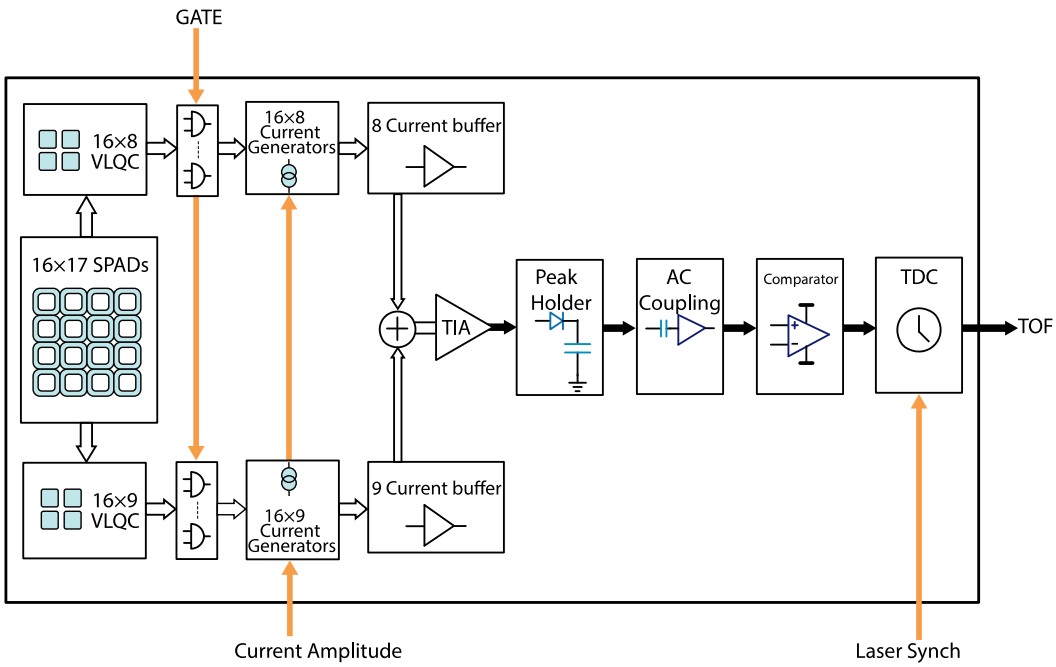

Fig. 2. Sensor chip architecture, with 272 SPADs driving 272 current sources, which add together so to provide an overall signal proportional to the number of concurrently detected photons within 5 ns coincidence time window; a Trans-Impedance Amplifier (TIA) feeds the peak detection circuitry, which tracks and holds the highest peak and triggers the TDC every time a new peak exceeds the one previously held, thus replacing its TOF value.

number of detected coincident photons, e.g., by summing all digital pulses. Then, a peak holder tracks this signal and holds the highest signal peak. A peak detector provides a pulse every time the peak holder tracks a signal higher than the previously held value.

For example, an AC-coupling stage can be used to provide the derivative of the peak holder output so to give a pulse at every incremental peak. The peak detector triggers a multi-hit TDC (e.g., a simple free-running counter), which overwrites the previous TOF with the new one (TOF 2 replaces TOF 1, in Fig. 1). At the end of the frame, before a next laser shot, only one TOF data will be available, which corresponds to the TOF of the highest signal peak detected within the desired Full-Scale Range (FSR) under investigation, i.e., the maximum distance.

Note that all the presented techniques require the signal to be higher than the background. The strong advantage of the rejection method that we are proposing is that it provides just the TOF of the signal peak containing the highest number of coincident photons. Since just one TOF is available in each frame, no further processing or data accumulation is needed, unlike TCSPC setups where a histogram has to be accumulated either on-chip (thus limiting SPAD array size or the spatial resolution, in case of more pixels) [16], [17] or off-chip (requiring high communication bandwidth and eventually limiting the achievable frame rate) [18]–[20].

III. Pixel Architecture

The chip we present is a single-pixel sensor for single-spot LiDAR acquisitions, capable of providing one TOF data per each laser-shot. The pixel can be exploited to reconstruct 3D depth-resolved maps by employing 2D scanning system. Since the pixel has been designed to cover an instantaneous FOV of 0.5°, it is possible to acquire a full 180°×50° scene at 1 MHz laser repetition rate and at 25 fps frame-rate. Higher frame-rates can be achieved with either fewer points or narrower total FOV.

Fig. 2 shows the chip architecture and building blocks, based on 272 SPADs connected in parallel so to sum together the photon detection events reducing the impact of background noise and saturation since signal photons are correlated in time while noise and ambient photons are randomly spread across the acquisition time. The electronics performs a digital-to-analog conversion from the digital pulses of each SPAD's quenching circuit to a total voltage waveform, proportional to the number of incoming photons. This analog signal is then processed by the on-chip analog electronics performing the peak detection technique described in Section II. A peak holder stores the highest peak detected since the last laser shot. An AC-coupling tracks the derivative of that signal, and a comparator triggers a multi-hit TDC to stores the TOF information whenever the new peek exceeds the previous one by one photon, i.e., the derivative signal gets higher than half a photon threshold. At the end of the frame, before the next laser shot, the only stored TOF value will be the last one, corresponding to the highest signal peak detected within the frame.

The sum of all detected photons, i.e., triggered SPADs, can be performed either in digital or in analog domain. In this implementation, due to the high number (272) of SPADs we preferred an analog solution since a digital logic would be bulkier. The SPAD detection events are converted into current pulses with adjustable amplitude and fixed 5 ns duration. The latter value sets the coincidence time window and is set to be equal to the pulse width of the employed laser. All current generators are grouped every 16 SPADs and each cluster is read by one of the

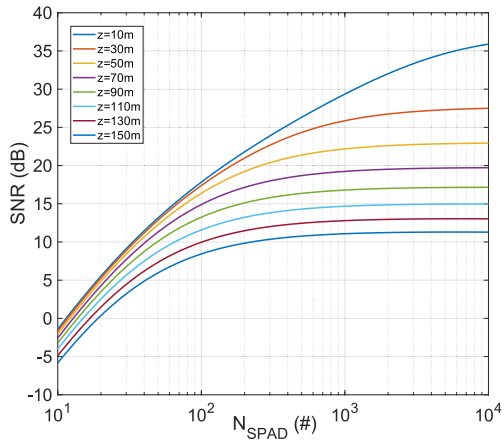

Fig. 3. Matlab simulations of the signal peak SNR, with an 80 W peak laser at 905 nm, 25% total efficiency (transmitter, receiver and filter), 0.5° × 0.5°FOV, 2 cm aperture and 100 klux background.

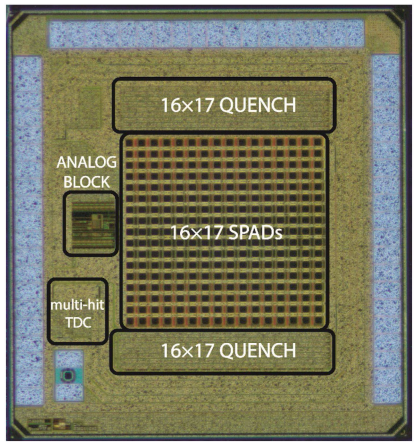

Fig. 4. Chip sensor micrograph and main building blocks. The chip dimensions are 2.00 mm × 2.15 mm, and the sensitive area is 1 mm × 1 mm.

17 current buffers. Such arrangement is necessary to equally distribute the parasitic capacitance of current generators and lines. Then, a transimpedance amplifier converts the total current into an analog voltage proportional to the number of concurrent photons hitting the SPADs. A double-stage peak tracker and holder and an AC-coupling stage drive the comparator to sense when the peak increases, so to temporary latch a multi-hit TDC into the single output storage cell. The TDC provides a 9-bit TOF information, with 2.5 ns resolution and about 1.28 μs FSR, corresponding to a single-shot distance resolution of 37.5 cm over a 192 m distance range.

A. SPADs and Pixel Architecture

The choice of the number of SPADs is dictated by the background level and the system optical parameters (such as FOV and optical aperture), since they all impact the photon rate on the sensor. Due to SPAD dead-time, a sub-set of available SPADs will be off when the laser echo reaches the active area; hence, the number of SPADs should be sufficiently high to have enough active SPADs to collect the signal photons.

In order to select the right number of SPADs, we have performed a numerical simulation to compute the signal to noise ratio (SNR) of the expected signal peak intensity compared to the ambient background, at different target distances and in the worst case condition of maximum reflectivity and 100 klux background level. The simulation has been carried out considering a 0.5° × 0.5° FOV, no limitation in chip area, and 80 W peak laser equally distributed over the active area. The SNR is computed as:

$$SNR = \frac{N_{ph,signal}}{\sqrt{N_{ph,signal} + N_{ph,background}}} \quad (1)$$

where $N_{ph,signal}$ and $N_{ph,background}$ are the number of concurrent detected photons, obtained as the sum of the SPAD digital pulses with 5 ns durations, computed as in the model described in [21]. Fig. 3 shows the simulation results: at low SPAD number, the background light saturates the SPAD array causing the SNR to drop; for an intermediate SPAD number, the SNR increases linearly; instead, increasing the number of SPADs beyond a certain number (dependent on target distance) does not significantly improve SNR. The reason being that photons become well distributed among all SPADs and saturation is no longer a problem. We selected 200 SPADs as a good trade-off between detector's pile-up (due to SPAD dead-time) and fill-factor (considering a given overall active area). For improving the performance at short distances, too many SPADs are required, resulting in a low fill-factor and complex on-chip processing even in the analog domain. Eventually, we embedded 272 (16×17) SPADs to leave some margin for disabling noisy pixels (with too high DCR) and matching the (usually round) shape of the laser spot.

The chip has been designed and fabricated in a 160 nm BCD technology [22]. Fig. 4 shows the 2.00 mm × 2.15 mm chip, with the 272 squared SPADs with 40 μm side each, occupying an overall active area of 1 mm × 1 mm in the center of the chip. The quenching circuits are all laid out outside the SPADs, to keep a high fill-factor (44%).

Each quenching circuit is a Variable Load Quenching Circuit (VLQC) similar to the one reported in [23], with a dead-time duration adjustable in the 10–200 ns range. The VLQC output digital pulse has an adjustable duration set to 5 ns to be equal to the laser's pulse width, since it defines the coincidence window.

B. Analog Adder

The pixel resembles an analog SiPM, where all the photons contribute to the global signal. However, in our implementation each microcell consists of a SPAD and a VLQC which provide a well-defined digital pulse of 5 ns duration at every photon detection [24]. Then each digital pulse drives a square-shaped current pulse, controllable in amplitude by an external reference voltage. All current generators are implemented by three 1.8V MOS transistors in series: the top one controls the current amplitude (from 20 μA to 80 μA); the bottom one turns the generator on/off; the middle one is driven by the GATE control signal and is used to gate on/off all SPADs so to enable synchronous detection only within specific time windows.

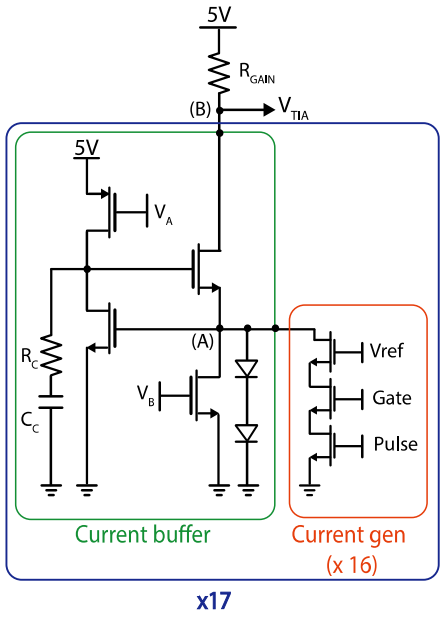

Fig. 5. Schematics of each current generator (right) and current buffer (left).

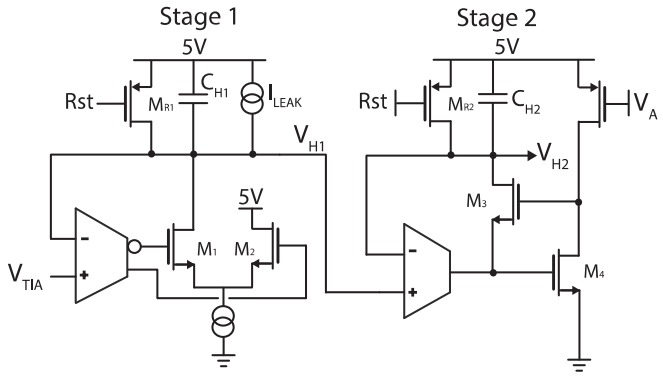

Fig. 6. Double-stage peak holder architecture.

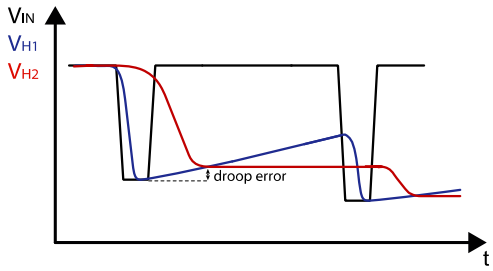

Fig. 7. Behavior of the double-stage peak holder.

The 272 current generators have been arranged in 17 groups of 16 devices each; this was necessary to lower the global capacitance at the summing node and to improve the analog bandwidth. Each one of the 16 current lines are read by one current buffer; then, the 17 current buffers sink their currents from a resistor to add all currents and output one voltage signal.

The 5 V current buffers have the feedback structure shown in Fig. 5. R_C and C_C are needed to improve stage stability by pushing the pole to low frequency and adding a negative zero, so to reach 1 GHz bandwidth. Particular care has been paid to the voltage range of node A, being the connection between 1.8 V and 5 V transistors. Two lightly forward bias diodes (few pA) have been added to clamp the rising of node A during power-on. The shared 500 Ω R_{GAIN} at node B provides a maximum dynamic range of 2 V, corresponding to 200 SPAD concurrently triggered, when the current sunk by each generator is set to the minimum value of 20 μA. The TIA electronic noise is about 300 μVrms, much less than the minimum signal of 10 mV per photon.

C. Peak Detector

The following analog block is meant to read the V_{TIA} voltage signal, to hold its peak value (V_H), and to provide a pulse every time a new peak exceeds the highest one detected so far in the present frame, i.e., since the last laser shot. The peak tracker and holder is composed by a transconductance amplifier and a non-linear component that turns on to charge a capacitor if $V_{TIA} < V_H$ or turns off otherwise.

The challenge in designing such a peak holder is to guarantee prompt tracking of multiple peaks within the 1 μs frame, because the detection of a second peak can be slower due to the recovery time of the components. Fig. 6 shows a double-stage implementation we conceived to solve the issue. The first stage is based on a current steering architecture with fast recovery and tracking behavior, thanks to a leaking current that weakly biases M_1, even if the output may droop. Instead, the second stage provides a stable peak hold, thanks to the complete turning off of M_3 and M_4 at the price of a lower bandwidth. Fig. 7 shows the behavior of the two stages: the first stage (blue trace) is fast but suffers of a large droop; instead, the second stage is slower, but catches the peak of the first one and hold it with negligible droop. The designed architecture is able to track 5 ns pulses of more than one photon each with less than 10% error and less than 4% if the peak consists of more than 3 photons. This performance is appropriate to the 5 ns Full-Width at Half Maximum (FWHM) target laser, while the fast background noise random coincidence peaks (i.e., about 1 ns width) are filtered out.

Transistors M_{R1} and M_{R2} are used to reset the peak holder at the end of the frame, just before the next laser shot. An AC-coupling and a comparator complete the analog chain. The former consists of a transimpedance amplifier driven by the peak holder through a series capacitor, which provides a charge current proportional to the V_{H2} derivative. The transimpedance architecture is similar to the one in Fig 5. (with no current generators) and it is designed using the 1.8 V supply rail needed by the following digital electronics. Finally, a comparator triggers as soon as the output of the AC-coupling block is greater than half a photon threshold.

D. TOF Timing Electronics

The proposed peak detection method requires to time-stamp all peaks detected by the peak detector and to overwrite the previously stored TOF value with the latest one. Thus, it is necessary to employ a multi-hit TDC with sufficiently long FSR, good resolution, and low dead-time among subsequent

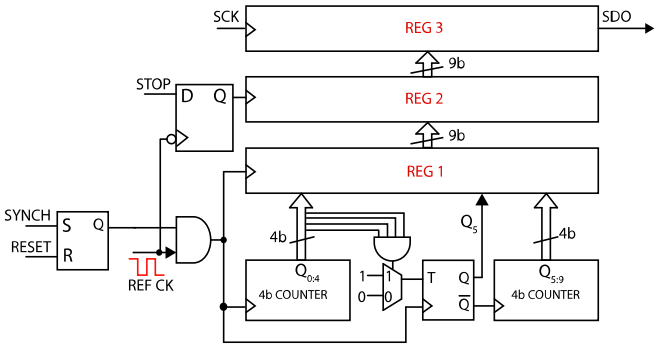

Fig. 8. Pseudo-synchronous ripple counter architecture for the TDC.

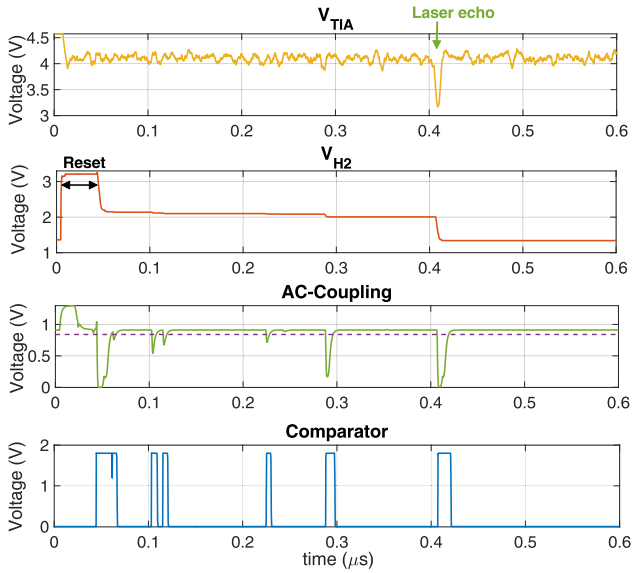

Fig. 9. Electrical simulations of the peak detection stages, for a 60 m distant object (400 ns TOF), 100 klux background light and 100% target reflectivity.

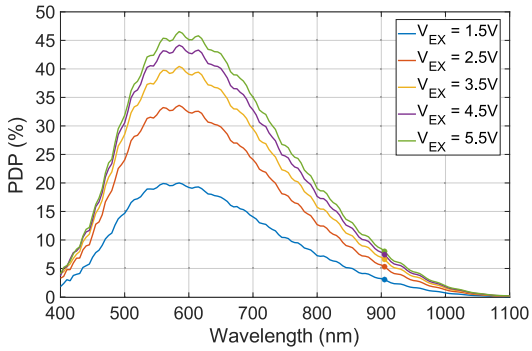

Fig. 10. Photon Detection Probability at different wavelength and excess bias.

conversions within the same frame. All these requirements are difficult to meet at once with one architecture; this is why some sensor chips for LiDAR sacrifice resolution to achieve longer ranges [17], [18].

We implemented a TDC based on a pseudo-synchronous ripple counter to provide long range, multi-hit feature, and nominal 2.5 ns resolution with a 400 MHz clock. The TDC can be clocked at 500 MHz achieving 2 ns resolution if a laser with a smaller FWHM is used.

Fig. 8 shows the TDC architecture: the counter is based on two 4 bits ripple counters and one bit resync toggle flip-flop. When the 4 least significant bits (LSBs) are digital "1s", the 5th bit toggles synchronous to the clock, thereby the 4 MSBs ripple after the clock rising-edge. This solution reduces the total counter propagation delay to 5 times the flip-flop one, instead of 9 (as in a full ripple-counter). The STOP signal (comparator output), after being synchronized to the inverted clock, samples the counter (latched every clock cycle in Reg 1) in Reg 2. If a new peak is detected (i.e., STOP is set high), the new TOF replaces the older one. The final TOF information is serially readout during the next frame in 9 clock cycles.

To better clarify the peak detection behavior, Fig. 9 shows a behavioral simulation of the circuit. The reset is needed at the beginning of every frame to discharge the peak holder capacitors. Every time a peak is detected, the comparator samples the TDC counter and store the new TOF value, so that the last trigger corresponds to the highest peak (the laser echo in the simulation) detected in the frame.

IV. Experimental Results

We developed a test board, with power supplies and data communication to a remote computer through an USB 3.0 link. The system is based on a commercial board (Opal Kelly XEM7310-A75) equipped with a Xilinx Artix-7 FPGA. The user can enable/disable each SPAD and adjust the SPAD pulse amplitude, depending on the specific application and the expected average number of (background and signal) photons.

In all measurements reported in the followings SPADs are operated at 3.5 V excess bias above breakdown, 400 MHz TDC clock, with 10 μA current pulses per SPAD (to exploit the whole dynamic range), if not differently specified.

The sensor consumes 400 mW when operated at high detection rate per SPAD (40/50 MHz), which corresponds to a very high background level.

A. SPAD Performance

We have characterized the SPAD performance in terms of Photon Detection Probability (PDP) and Dark Count Rate (DCR). Fig. 10 shows the PDP vs. wavelength: at 3.5V excess bias, the PDP reaches 41% at 590 nm and decreases to 6.7% at 905 nm, target wavelength for our LiDAR system. At 5V excess bias, these values increase to 46% and 8%, respectively. Fig. 11 shows the DCR at different chip temperatures. During standard operation, the average chip temperature was 40°C, with a median DCR of 18 kcps (counts per second) and just 11% of pixels with a DCR higher than two times the median one.

B. Pixel Performance

The timing performance of SPADs and front-end electronics have been characterized by illuminating the array with a pulsed laser (with 400 ps resolution and 850 nm wavelength by ALS) and acquiring the current signal from a single SPAD by means

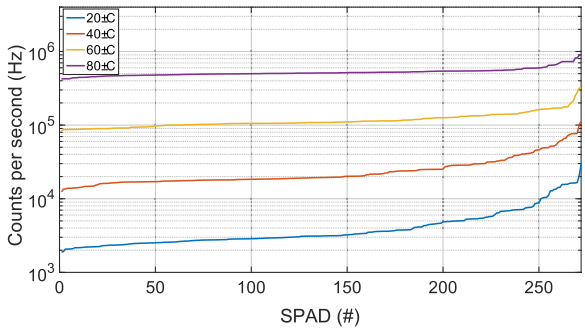

Fig. 11. Dark Count Rate sorted per increasing values, at different temperatures.

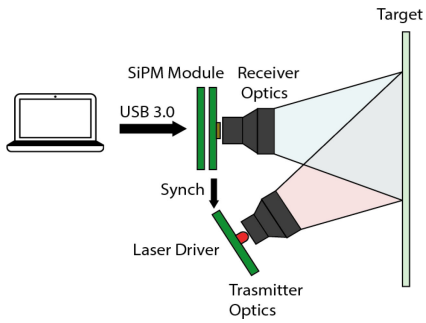

Fig. 12. Preliminary setup for outdoor distance measurements.

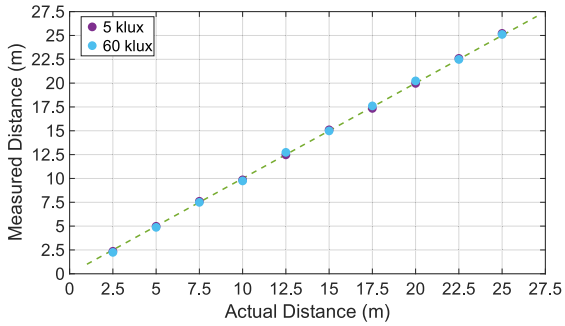

Fig. 13. Measured distance vs. actual ground-true distance in outdoor acquisitions, at two different environmental conditions of 5 klux (cloudy day) and 60 klux (sunny autumn day).

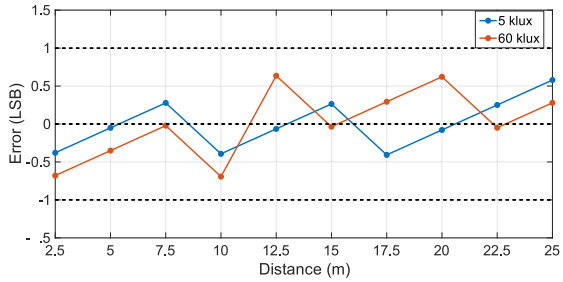

Fig. 14. Distance error of Fig. 13 data compared to the resolution limit of the TDC Least Significant Bit (2.5 ns), at 5 klux and 60 klux background.

of a TCSPC board (SPC-630 by Becker&Hickl GmbH). The resulting histogram has a FWHM of 260 ps, significantly better than the 2.5 ns target resolution, mostly limited by the pulsed laser selected for the LiDAR system.

Having placed the VLQC electronics outside the SPAD array maximizes the FF but causes a mismatch in the length of anode connections between SPADs and VLQCs. In order to achieve a better matching of the metal paths (hence of the capacitive loads), the closest VLQC blocks have been connected to the inner SPADs. In this way, the worst skew measured among the most distant SPADs is 45 ps, definitely negligible. Optical crosstalk can cause coincidence events not due to signal photons, but to spurious SPADs triggering due to secondary photons emitted by a primary avalanching SPAD [25].

To characterize the optical crosstalk, we kept the camera in a dark environment, we activated selected couples of SPADs and we monitored the triggering of an external comparator connected to the chips' common analog output, with a threshold equivalent to two photons. Considering the accidental coincidences due to the two SPADs DCRs ($\mathrm{R_A}$ and $\mathrm{R_B}$) in a 5 ns time window are negligible (in the order of 4 coincidence/s for two not noisy SPADs) all the measured events ($\mathrm{R_{coinc}}$) can be considered crosstalk events. Then, the crosstalk probability ($\mathrm{P_{AB}}$) can be calculated as:

$$P_{\mathrm{AB}}=\frac{\mathrm{R_{coinc}}}{\mathrm{R_A}+\mathrm{R_B}} \tag{2}$$

For two neighboring pixels, the measured crosstalk probability is 1.25% for orthogonal SPADs and 0.1% for oblique ones.

C. Preliminary Validation

In order to validate the actual background rejection and the TOF performance of the chip, we performed acquisitions in an outdoor LiDAR scenario, with the setup shown in Fig. 12. We used a non-coaxial configuration, employing a laser with 6 ns FWHM and 25°×9° divergence. The laser diode was at 905 nm (SPL PL90_3 by OSRAM Opto Semiconductors), driven by a commercial board (EPC9126HC by EPC), then reshaped to obtain a 2.3°×2.3° divergence and 6 mW average output power. The repetition rate was set to 100 kHz, limited by the laser driver. Instead, the final system will employ a 5-ns FWHM pulsed laser, with 0.5°×0.5° divergence, coaxial with the detector, together with a scanning mechanism. At present, the laser driver and the optics are under development.

Since the preliminary setup is not optimized for the chip specifications, the receiver optics has been chosen to increase the signal collection, bringing the FOV from the nominal value to 0.76°×0.76° (f/1.8, 75 mm focal length). The measured background levels of 5 klux and 60 klux correspond to a cloudy and a sunny autumn day in Milan, respectively. Before the receiver, we placed an optical bandpass filter, centered at 905 nm wavelength and with a 25 nm FWHM.

We repeated 200000 single-shot measurements for each distance to verify the reliability of the single-shot acquisitions by observing the success ratio, defined as $\frac{\#\ correct\ TOFs}{\#\ total\ TOFs}$. The most frequent value for each distance and background level is plotted in Fig. 13 vs. the ground-true distance. Fig. 14 shows the difference between real and measured distance: note that the maximum error does not exceed 1 LSB, equal to 37.5 cm.

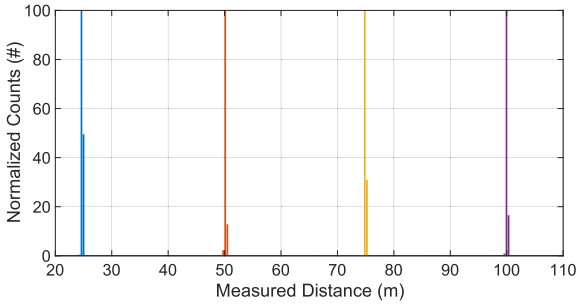

Fig. 15. Example of multiple acquisitions to determine the success of single-shot measurements, at 25 m, 50 m, 75 m, 100 m distance.

TABLE I
SUMMARY OF THE SINGLE-SHOT MEASUREMENTS

Max Distance	Environment	Background	Success
25 m	Outdoor	5 klux	99%
25 m	Outdoor	60 klux	95.4%
150 m	Indoor	100 lux	93%
150 m	Indoor	10 klux	50%

We computed the success ratio of each single-shot measurement, as the ratio between the counts in the highest bin of the collected TOF histogram and its neighbor and the sum of all the events, as the example in Fig. 15 shows. An event is considered "a success" if it falls either in the main bin or its highest neighbor, the reason being that the laser FWHM (6 ns) is larger than the TDC's LSB (2.5 ns). At 25 m, the success ratio is 99% at 5 klux background and 95.4% at 60 klux background.

A non-coaxial setup is suboptimal since the spot changes position at every distance requiring a manual reposition of the optics. Furthermore, the available outdoor space exposed to sunlight was only 27 m longer. Thus, in order to better verify the chip capability, we performed various indoor acquisitions.

To mimic the signal power degradation due to distance ($\propto \frac{1}{z^2}$), the laser has been attenuated using combinations of Neutral-Density (ND) filters. The different returning time delays of the laser echo at the various distances have been emulated by adding a variable delay between the TDC start signal and the laser trigger. A background of about 10 klux has been generated through a fixed halogen light source, since it does not depend on the target distance. The acquisitions cover a range of 150 meters in 100 lux (no halogen light) and 10 klux background situations.

We employed the same optics, laser emitter, and post-processing as in the outdoor measurements. Figs. 16 and 17 show the measured distances and the error respectively. The error shows a periodical pattern due to the quantization error of the TDC and the measurement steps of 5 meters (10 meters from 100 m on).

Fig. 18 shows the error considering, instead of the TOF of the highest peak, the centroid of the histogram (weighted average of the two highest bins), to highlight the error trend on the measurement. It can be noticed the TOF anticipation at shorter distances, due to the pile-up distortion, while at longer distances the walk error produces higher TOF, since the echo peak is

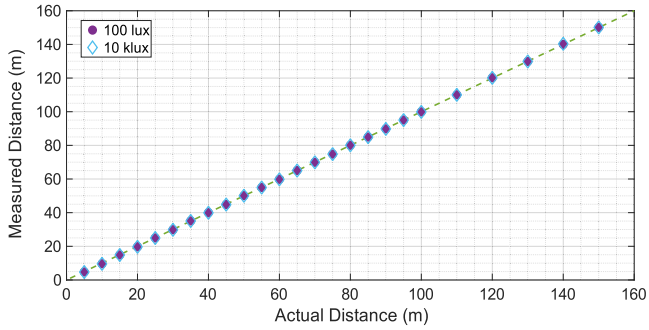

Fig. 16. Measured distance vs. actual ground true distance in indoor acquisitions, at two different environmental conditions of 100 lux and 10 klux.

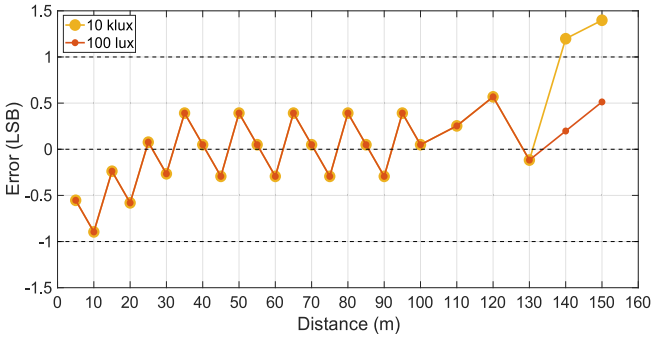

Fig. 17. Distance error of Fig. 16 data compared to the resolution limit of the TDC's Least Significant Bit (2.5 ns), at 100 lux and 10 klux of background illumination.

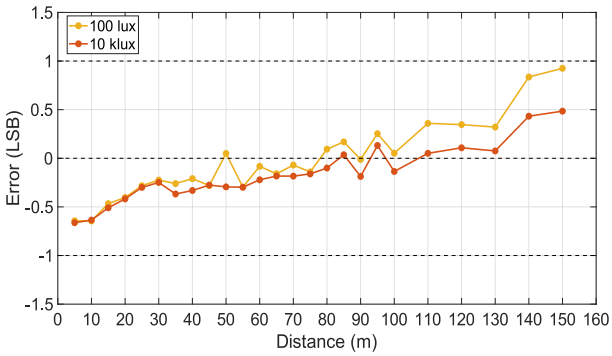

Fig. 18. Distance error of Fig. 16 data compared to the resolution limit of the TDC's Least Significant Bit (2.5 ns), at 100 lux and 10 klux of background illumination, computed as the centroid of the resulting histogram.

weaker and the electronics delay increases. This trend is less evident in the outdoor measurements, due to shorter distances and a not-perfect alignment of the optics. In the worst case, in a 150 m range the error spreads from -0.6 to about 1 LSB.

We have obtained a success ratio higher than 97% for both background levels within the 5–130 m range. At 150 m we get a 93% success at 100 lux background and 50% at 10 klux. The precision and the success can be affected by the AC-coupling recovery time. Observing Fig. 9, it is possible to notice that if a noise peak is detected by the AC-coupling some ns before the signal peak, this stage can take some time to recover and the comparator would trigger only in correspondence of the noise, without providing another pulse in correspondence to the laser

TABLE II
COMPARISON OF THE MAIN PERFORMANCE PARAMETERS AMONG STATE-OF-ART SINGLE-SPOT LIDAR SPAD ARRAYS

	This work	[9]	[26]	[27]
Sensor characteristics				
Process	**160 nm**	160 nm	150 nm	350 nm HV
Approach	**Single-shot peak detection**	ROI detection	ROI detection	Time-gating
Array size	**16×17**	40×10	50×40	9×9
Chip size	**2×2.15 mm^2**	2.73×3.37 mm^2	3.3×2.9 mm^2	2.5×4 mm^2
Pixel fill factor	**44%**	14%	15.3%	50%
N TDC	**1**	80	25	10
Resolution	**2 ns**	78 ps	40.7 ps	65 ps
Range	**154 m**	2.2 m	7.5 m	80 m
Power	**400 mW**	200 mW	28.3 mW	-
Emitted parameters				
Wavelength	**905 nm**	670 nm	470 nm	810 nm
Power	**6 mW**	14 µW	40 µW	50 µW
Repetition rate	**100 kHz**	1 MHz	10 MHz	100 kHz
Optics parameters				
FOV	**0.76°×0.76°[(1)]**	1.1°×4.5°[(1)]	-	0.043°×0.043°[(1)]
Lens focal length	**75 mm**	12 mm	-	40 mm
Lens aperture	**42 mm**	8.57 mm	-	20 mm
Optical filter bandwidth	**25 nm**	10 nm	50 nm	50 nm
LiDAR measurements				
Maximum measured range	**25 m[(2)], 150 m[(3)]**	2 m	3 m	73.2 m[(4)]
Maximum background	**60 klux[(2)], 10klux[(3)]**	10 klux	18 klux	90 klux
Precision (background)	**37.5 cm[(5)](60 klux)**	2.3 mm (3 klux)	1.6 mm (7 klux)	20 mm (50 lux)

[(1)]The activated SPADs illuminated by the laser; [(2)]Outdoor measurement; [(3)]Indoor measurements; [(4)]Gate opened 25 ns before object; [(5)]The TDC was configured with 2.5 ns resolution.

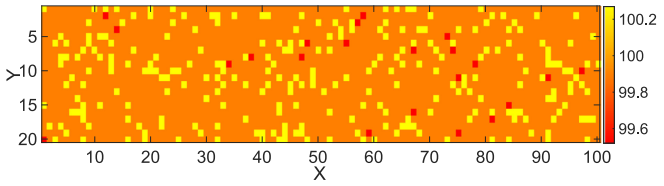

Fig. 19. 2000 single-shots acquisitions at 10 klux background illumination at 100 m distance.

peak. This can be noticed in the small peak before the highest one in Fig. 15, corresponding to about 4% of the events in that condition.

Finally, we performed 2000 single-shot measurements at the same conditions of Fig. 16. Measured distance vs. actual ground true distance in indoor acquisitions, at two different environmental conditions of 100 lux and 10 klux. (10 klux) and attenuated laser to emulate an object at 100 m. The 2000 ToFs have been re-organized as 20×100 map, as shown in Fig. 19, to better appreciate the uniformity. We can notice that two main distances appear (100.265 m and 99.9 m) since the laser FWHM is wider than 2 bins. The wrong TOFs are less than the 3%.

V. CONCLUSION

We have presented a novel background rejection method that enables single-shot LiDAR measurements in outdoor applications under high ambient background noise. When compared with architectures based on TCSPC techniques TOF histogram collection, the proposed single-shot chip reduces the acquisition time per point, which is one of the major limitations in scanning LiDAR systems.

The chip embeds 272 SPADs and analog electronics that sums all concurrent photons and measures the TOF of the highest peak detected per each laser shot. The target FOV is 0.5°×0.5°, for acquiring 36'000 points in a 180°×50° scanned scene, with a 1 MHz laser repetition rate and 25 fps frame-rate. Chip performance have been optimized for a 5 ns FWHM laser pulse at 905 nm and with 80 W peak. The chip integrates a 2 ns resolution multi-hit TDC with 1 μs FSR and SPADs with 6.7% PDP at 905 nm and negligible DCR and crosstalk.

We validated the chip performance and the background rejection method through a preliminary setup, achieving 95.4% success ratio in single-shot TOF measurements at 25 m with 60 klux background. We are developing the final setup, with the proper optics used to size the chip, in order to operate at longer distances (up to 150 m), with a coaxial system for 0.5°×0.5°FOV. Indeed, employing a non-coaxial setup requires aligning the laser spot with the detection optics, procedure that can compromise the collected laser signal above all at longer distances, thus reducing SNR. Indoor measurements proved the reliability of the device up to 140 m with 10 klux background. These results are summarized in Table I.

Considering the pixel dimension, replicating its structure in a 2D array is not feasible. However, starting from the proposed pixel, it is possible to design a 1D imager to have multi-point acquisitions. In order to reduce the chip area, it is possible to choose a lower number of SPADs per pixel, decreasing accordingly the instantaneous FOV not to saturate in high background conditions.

TABLE II shows a comparison between other single-point SPAD arrays. It can be noticed that our array provides a coarser time resolution, but it achieves long range, provides background rejection, and is the only one that allows single-shot measurements and employs just one TDC without requiring post-processing, since it generates only the TOF related to the peak, which can be read in 9 clock periods.

REFERENCES

[1] S. Hussmann, T. Ringbeck, and B. Hagebeuker, "A performance review of 3D TOF vision systems in comparison to stereo vision systems," in *Stereo Vision*. London, U.K.: IntechOpen, 2008, pp. 103–119.

[2] H. Ruokamo, L. W. Hallman, and J. Kostamovaara, "An 80×25pixel CMOS single-photon sensor with flexible on-chip time gatingof 40 subarrays for solid-state 3-D range imaging," *IEEE J. Solid-State Circuits*, vol. 54, no. 2, pp. 501–510, Feb. 2019.

[3] G. Zhou *et al.*, "Flash LiDAR sensor using fiber-coupled APDs," *IEEE Sensors J.*, vol. 15, no. 9, pp. 4758–4768, Sep. 2015, doi: 10.1109/JSEN.2015.2425414.

[4] S. W. Hutchingset *et al.*, "A reconfigurable 3-D-stacked SPAD imager within-pixel histogramming for flash LiDAR or high-speed time-of-flight imaging," *IEEE J. Solid-State Circuits*, vol. 54, no. 11, pp. 2947–2956, Nov. 2019.

[5] G. Adamo *et al.*, "Time of flight measurements via two LiDAR systems with SiPM and APD," in *Proc. AEIT Int. Annu. Conf.*, 2016, pp. 1–5.

[6] M. Renna *et al.*, "High detection rate fast-gated CMOS single-photon avalanche diode module," *IEEE Photon. J.*, vol. 12, no. 5, Oct. 2020, Art. no. 6802312. doi: 10.1109/JPHOT.2020.3017092.

[7] A. Tosi, N. Calandri, M. Sanzaro, and F. Acerbi, "Low-noise, low-jitter, high detection efficiency InGaAs/InP single-photon avalanche diode," *IEEE J. Sel. Topics Quantum Electron.*, vol. 20, no. 6, Nov./Dec. 2014, Art. no. 3803406.

[8] W. Becker, *The bh TCSPC Handbook*, 9th ed. Berlin, Germany: Becker & Hickl, 2021. [Online]. Available: www.becker-hickl.com

[9] V. Sesta *et al.*, "Spot tracking and TDC sharing in SPAD arrays for TOF LiDAR," *Sensors*, vol. 21, no. 9, 2021, Art. no. 2936. doi: 10.3390/s21092936.

[10] R. Agishev *et al.*, "LiDAR with SiPM: Some capabilities and limitations in real environment," *Opt. Laser Technol.*, vol. 49, pp. 86–90, 2013.

[11] P. Organtini *et al.*, "Industrial exploitation of SiPM technology developed for basic research," *Nucl. Instrum. Methods Phys. Res. Sect. A*, vol. 978, 2020, Art. no. 164410, doi: 10.1016/j.nima.2020.164410.

[12] W. Becker, *Advanced Time-Correlated Single Photon Counting Techniques*. Berlin, Germany: Springer-Verlag, 2005.

[13] B. Joly, G. Montarouand, and P. Vert, "Sampling rate and ADC resolution requirements in digital front-end electronics for TOF PET," *IEEE Trans. Nucl. Sci.*, vol. 64, no. 9, pp. 2543–2550, Sep. 2017, doi: 10.1109/TNS.2017.273203.

[14] C. S. Bamji *et al.*, "A 0.13 μm CMOS system-on-chip for a 512 × 424 time-of-flight image sensor with multi-frequency photo-demodulation up to 130 MHz and 2 GS/S ADC," *IEEE J. Solid-State Circuits*, vol. 50, no. 1, pp. 303–319, Jan. 2015.

[15] P. Palojarvi, T. Ruotsalainen, and J. Kostamovaara, "A 250-MHz BiCMOS receiver channel with leading edge timing discriminator for a pulsed time-of-flight laser rangefinder," *IEEE J. Solid-State Circuits*, vol. 40, no. 6, pp. 1341–1349, Jun. 2005.

[16] H. Seo *et al.*, "Direct TOF scanning LiDAR sensor with two-step multievent histogramming TDC and embedded interference filter," *IEEE J. Solid-State Circuits*, vol. 56, no. 4, pp. 1022–1035, Apr. 2021.

[17] S. W. Hutchings *et al.*, "A reconfigurable 3-D-stacked SPAD imager with in-pixel histogramming for flash lidar or high-speed time-of-flight imaging," *IEEE J. Solid-State Circuits*, vol. 54, no. 11, pp. 2947–2956, Nov. 2019.

[18] C. Niclass, M. Soga, H. Matsubara, S. Kato, and M. Kagami, "A 100-m range 10-frame/s 340×96-pixel time-of-flight depth sensor in 0.18-μm CMOS," *IEEE J. Solid-State Circuits*, vol. 48, no. 2, pp. 559–572, Feb. 2013.

[19] M. Perenzoni, D. Perenzoni, and D. Stoppa, "A 64 x 64-pixels digital silicon photomultiplier direct TOF sensor with 100-mphotons/s/pixel background rejection and imaging/altimeter mode with 0.14% precision up to 6 km for spacecraft navigation and landing," *IEEE J. Solid-State Circuits*, vol. 52, no. 1, pp. 151–160, Jan. 2017.

[20] A. R. Ximenes *et al.*, "A modular, direct time-of-flight depth sensor in 45/65-nm 3-D-stacked CMOS technology," *IEEE J. Solid-State Circuits*, vol. 54, no. 11, pp. 3203–3214, Nov. 2019.

[21] A. Incoronato, M. Locatelli, and F. Zappa, "Statistical modelling of SPADs for time-of-flight LiDAR," *Sensors*, vol. 21, no. 13, 2021, Art. no. 4481.

[22] M. Sanzaro *et al.*, "Single-photon avalanche diodes in a 0.16 μm BCD technology with sharp timing response and red-enhanced sensitivity," *IEEE J. Sel. Topics Quantum Electron.*, vol. 24, no. 2, Mar./Apr. 2018, Art. no. 3801209.

[23] D. Portaluppi, E. Conca, and F. Villa, "32 × 32 CMOS SPAD imager for gated imaging, photon timing, and photon coincidence," *IEEE J. Sel. Topics Quantum Electron.*, vol. 24, no. 2, Mar./Apr. 2018, Art. no. 3800706.

[24] C. Niclass, M. Soga, and S. Kato, "A 0.18μm CMOS single-photon sensor for coaxial laser rangefinders," in *Proc. IEEE Asian Solid-State Circuits Conf.*, 2010, pp. 1–4, doi: 10.1109/ASSCC.2010.5716568.

[25] A. Ficorella *et al.*, "Crosstalk mapping in CMOS SPAD arrays," in *Proc. 46th Eur. Solid-State Device Res. Conf.*, 2016, pp. 101–104.

[26] M. Perenzoni *et al.*, "A fast 50 × 40-pixels single-point DTOF SPAD sensor with photon counting and programmable ROI TDCS, with σ<4mm at 3 m up to 18 klux of background light," *IEEE Solid-State Circuits Lett.*, vol. 3, pp. 86–89, 2020.

[27] J. Huikari, S. Jahromi, J.-P. Jansson, and J. Kostamovaara, "Compact laser radar based on a subnanosecond laser diode transmitter and a two-dimensional CMOS single-photon receiver," *Opt. Eng.*, vol. 57, no. 2, 2018, Art. no. 024104.

Alfonso Incoronato (Graduate Student Member, IEEE) was born in Segrate, Italy, in 1994. He received the B.Sc. degree in biomedical engineering and the master's degree in electronics engineering from Politecnico di Milano, Milano, Italy, in 2016 and 2019, respectively, where he has been working toward the Ph.D. degree in information technology (electronics) since November 2019. His research activities include the microelectronic design of SPADs and SiPM arrays for automotive LiDAR.

Iris Cusini was born in Tirano, Italy, in 1994. She received the B.Sc. degree in automation engineering (*summa cum laude*) from Politecnico di Milano, Milano, Italy, and Tongji University, Shanghai, China, within a double degree project, and the M.Sc. degree (*summa cum laude*) in electronics engineering in 2019 from Politecnico di Milano, where she has been working toward the Ph.D. degree in information technology since November 2019. Her research interests include the design, development, and testing of systems with single-photon avalanche diodes and digital silicon photomultipliers.

Klaus Pasquinelli was born in Seriate, Italy, in 1994. He received the B.Sc. and M.Sc. degrees in electronics engineering in 2016 and October 2018, respectively, from Politecnico di Milano, Milano, Italy, where he has been working toward the Ph.D. degree in information technology since November 2018. His research interests include the design, development, and testing of systems with single-photon avalanche diodes matrices and digital silicon photomultiplier.

Franco Zappa (Senior Member, IEEE) was born in Milano, Italy, in 1965. Since 2011, he has been a Full Professor of electronics with Politecnico di Milano, Milano, Italy. His research interests include microelectronic circuitry for single-photon detectors (SPAD) and CMOS SPAD imagers, for high-sensitivity time-resolved measurements, 2D imaging, and 3D depth ranging. In 2004, he co-founded "Micro Photon Devices," producing SPAD modules and cameras for single photon-counting and photon-timing, and in 2020 pioNIRS, developing near-infrared spectroscopy instrumentation for non-invasive and continuative monitoring of biological tissues and food.